EFFECTIVE CONTROL OF COMPUTATIONALLY SIMULATED WING ROCK IN SUBSONIC FLOW

Osama A. Kandil* and Margaret A. Menzies**
Aerospace Engineering Department
Old Dominion University, Norfolk, Virginia 23529

ABSTRACT

The unsteady, compressible, full Navier-Stokes (NS) equations and the Euler equations of rigid-body dynamics are sequentially solved to simulate the delta wing rock phenomenon. The NS equations are solved time accurately using the implicit, upwind, Roe flux-difference splitting, finite-volume scheme. The rigid-body dynamics equations are solved using a four-stage Runge-Kutta scheme. Once the wing reaches the limit-cycle response, an active control model using a mass injection system is applied from the wing surface to suppress the limit-cycle oscillation. The active control model is based on state feedback and the control law is established using pole placement techniques. The control law is based on the feedback of two states; the roll-angle and roll velocity. The primary model of the computational applications consists of a 80° swept, sharp edged, delta wing at 30° angle of attack in a freestream of Mach number 0.1 and Reynolds number of 0.4×10^6. With a limit-cycle roll amplitude of 41.1°, the control model is applied, and the results show that within one and one half cycles of oscillation, the wing roll amplitude and velocity are brought to zero.

INTRODUCTION

One frequently encountered lateral instability which limits combat effectiveness for all fighter aircraft is the limit-cycle rolling oscillation phenomenon known as wing rock. In moderate to high angle-of-attack dynamic motion, wing rock is driven by strong, concentrated vortices originating from the leading edges of highly swept wings. Wing rock can occur at subsonic airspeeds at angles of attack in the vicinity of stall and at moderate angles of attack in the transonic regime as a result of shock-wave/boundary-layer interactions on the wing. Generally, the onset of wing rock can be caused by a number of different aerodynamic phenomena and is attributed to a loss of stability in the lateral/directional mode.

To understand the wing rock phenomenon, experimental investigations have been carried out on simplified delta-wing geometries with a single degree of freedom in roll. By avoiding the complexity of complete aircraft geometries, research can focus on the relevant flow physics. Experimental data typically consists of flow visualization, time-dependent forces and moments and more recently, time-dependent surface pressure data. The time-dependent pressure data provides additional information that allows for more detailed understanding of the mechanisms involved with wing rock which have yet to be fully understood. However, these experimental results are limited by the difficulties encountered in taking measurements in a dynamic environment.

Computational fluid dynamics (CFD) plays an important role in the design process by providing detailed flowfield information at a relatively low cost that is unavailable with experiment alone. It helps reduce design cycle time and provides information that is complementary to wind-tunnel and flight-test data. With recent advances in computer hardware, system software and numerical methods, multidisciplinary studies have emerged which afford maximum potential benefits from limited resources. A few computational studies have been initiated to simulate the wing rock problem. However, due to large amounts of computational time, most of these studies have employed various limiting approximations to reduce the computational cost. Inherently, these simplifying flow assumptions restrict the applicability of the solution to steady or inviscid flows. For vortical flows where viscous effects dominate, computation based on the unsteady Navier-Stokes equations is vital. The Navier-Stokes equations can more accurately model flow separations, shock development and motion, and shock-boundary-layer interaction as well as vortex breakdown and vorticity evolution, convection and shedding.

In 1981, the phenomena of slender wing rock was first observed in experiments performed by Nguyen, *et al.*[1] Using an 80° swept delta wing investigation showed that wing rock occurred simultaneously with the appearance of asymmetric leading-edge vortices. By 1984, Ericsson[2] had shown that vortex asymmetry could generate wing rock but growth of the amplitude was limited by vortex breakdown. Arena[3] conducted a thorough experimental investigation of the natural response of a slender wing rock in subsonic flow. He identified the envelope of damped and self sustaining motion for an 80° swept wing and qualitatively compared these results with computational results. Continuing investigation of wing rock, Ng, *et al.*,[4] used a water tunnel to compare forced rolling and free-to-roll oscillations of delta wings of various sweep angles with static conditions.

Various experimental attempts to control wing rock have also been investigated experimentally. Malcolm, *et al.*[5] demonstrated a wing's rolling moment can be affected by mechanical or pneumatic manipulation of the strength or location of the leading-edge vortices. In 1993, Walton and Katz[6] exploited this idea and applied leading edge control flaps to a free-to-roll double-delta wing. In 1994, Ng, *et al.*,[7] demonstrated passive control of an 80° swept delta wing undergoing wing rock by using flow dividers. At angles of attack higher than 30°, suppression of wing rock was achieved. However, at lower angles of attack, the divider actually promoted the phenomenon. Using asymmetric tangential leading-edge blowing, Wong, *et al.*,[8] demonstrated positive post-stall roll control for a delta wing at an angle of attack of 55°. With an active roll feedback

*Professor, Eminent Scholar and Department Chairman, Associate Fellow AIAA.

**Ph.D. Research Assistant, Currently Staff Engineer with Avionics Specialists, Charlottesville, VA, Member AIAA.

control algorithm employing a proportional-derivative compensator, wing rock was stopped in less than one cycle of the limit-cycle motion.

As in experimental investigations of forced rolling oscillations, the focus of computational studies is to be able to predict and ultimately control the phenomenon of wing rock. In 1985, using an unsteady vortex-lattice method, Konstadinopoulos, *et al.*[4] numerically simulated the subsonic experimental work performed by Nguyen, *et al.*[1] They determined that the leading-edge vortex system became unstable as the angle of attack was increased which caused a loss of roll damping at small angle of roll. Improving the methods for numerical simulation, in 1989, Nayfeh, *et al.*[10] proceeded to construct phase planes which revealed the general global nature of wing rock by discussing stable limit cycles, unstable foci, and saddle points. This demonstrated the locations of equilibrium positions. By 1994, Chaderijian and Schiff *et al*[11] had solved for flow over a 65° swept delta wing at 30° angle of attack and Mach of 0.27 that was both forced and free to roll under the influence of the instantaneous aerodynamic rolling moment.

Numerical simulation for the control of wing rock has been performed by various authors primarily using Euler equations assuming locally conical flow. In 1991, after developing the Navier-Displacement equations for grid deformation, Kandil and Salman[12] effectively controlled the wing rock response of an 80° swept delta wing at 30° angle of attack and Mach number of 1.2 by using tuned antisymmetric leading-edge flap oscillations. They later applied the locally conical Euler equations to the same problem at Mach 1.4. The three-dimensional flow solution of Euler equations at Mach 0.3 were also considered.[13] Noting the loss of aerodynamic damping rolling moment at the zero angular velocity value, they determined that the hysterias responses of position and strength of the asymmetric right and left primary vortices were responsible for wing rock and that the phenomenon could be actively controlled through the use of leading edge flaps. In 1991, Kandil and Salman[14] solved the thin-layer locally conical Navier-Stokes equations for delta wing at 35° angle of attack. It was again showed that the wing-rock phenomenon could be controlled by using tuned anti-symmetric leading-edge flap oscillations. Details of this work were published in Salman's dissertation.[15] In 1993, Lee-Rausch and Batina[16] also investigated control of wing rock using locally conical Euler equations using leading-edge flaps. Their study focused on a 75° swept sharp-edged delta wing at a free-stream Mach number of 1.2 at various angles of attack.

In Ref. 17, Menzies and Kandil presented three cases of computationally simulated natural rolling response of a delta wing in transonic and subsonic flow. This was the only known published study in the transonic flow regime using the NS equations. Transonic flow over a 65° swept, cropped delta wing with breakdown of the leading edge vortices demonstrated self sustained rolling oscillations until breakdown dominates the flow field. Two cases of subsonic flow over an 80° swept wing demonstrated either damped or self-sustained rolling oscillations as a function of angle of attack. A complete investigation of the aerodynamic response of the wing, the effects of Mach number, angle of attack, and vortex breakdown are presented.

In this paper, an active control model using a mass injection system is developed and applied to a delta wing undergoing 41.1° rolling amplitude of self-sustained limit cycle response. The model is based on state feedback and the control law is established using pole placement technique. The state feedback is designed for the feedback of two states: the roll angle and roll velocity.

FORMULATION OF WING ROCK PROBLEM

Governing Equations:

The conservative form of the dimensionless, unsteady, compressible, full Navier-Stokes equations in terms of the time-dependent, body-conformed coordinates ξ^1, ξ^2, and ξ^3, is given by:

$$\frac{\partial \overline{Q}}{\partial t} + \frac{\partial \overline{E}_m}{\partial \xi^m} - \frac{\partial (\overline{E}_v)_s}{\partial \xi^s} = 0; \quad m = 1,2,3; \quad s = 1,2,3 \qquad (1)$$

where

$$\xi^m = \xi^m(x_1, x_2, x_3, t) \qquad (2)$$

$$\overline{Q} = \frac{\hat{q}}{J} = \frac{1}{J}[\rho, \rho u_1, \rho u_2, \rho u_3, \rho e]^t \qquad (3)$$

The definitions of the inviscid and viscous fluxes; $\overline{E}_m$ and $(\overline{E}_v)_s$ are given in Ref. 18.

To achieve the natural response of the wing to the fluid flow, the wing motion is obtained by coupling the fluid dynamics with rigid body dynamics. The resultant external aerodynamic rolling moment, $C_{m_{roll}}$, is equated to the time rate of change of the angular momentum vector about the axis of rotation as follows:

$$C_{m_{roll}} = I_{xx}\dot{\omega}_x + (I_{zz} - I_{yy})\omega_y\omega_z \qquad (4)$$

where I_{ii} are the principal mass moments of inertia for the wing, ω_x is the rolling velocity, and ω_y and $\omega_z = 0$ for single degree of freedom motion (rolling motion).

Boundary And Initial Conditions and Grid Motion

All boundary conditions are explicitly implemented. They include inflow-outflow conditions, solid-boundary conditions and plane of geometric symmetry conditions. At the plane of geometric symmetry, periodic conditions are enforced. At the inflow boundaries, the Riemann-invarient boundary-type conditions are enforced. At the outflow boundaries, first-order extrapolation from the interior point is used.

Since the wing is undergoing rolling motion, the grid is moved with the same angular motion as that of the body. The grid speed, $\frac{\partial \xi^m}{\partial t}$, and the metric coefficient, $\frac{\partial \xi^m}{\partial x_n}$, are computed at each time step of the computational scheme. Consequently, the kinematic boundary conditions at the inflow-outflow boundaries and at the wing surface are expressed in terms of the relative velocities. The dynamic boundary condition, $\frac{\partial p}{\partial n}$, on the wing surface is no longer equal to zero. This condition is modified for the oscillating wing as:

$$\left.\frac{\partial p}{\partial n}\right|_{wing} = -\rho\, \vec{a} \cdot \hat{n} \qquad (5)$$

where $\vec{a}$ is the acceleration of a point on the wing flat surface; $\hat{n}$, the unit normal to the wing surface which is equal to the unit vector $\bar{e}_z$ for a flat surface. The acceleration is given by:

$$\vec{a} = \dot{\vec{\Omega}} \, x \, \vec{r} + \vec{\Omega} \, x \left(\vec{\Omega} \, x \, \vec{r} \right) \tag{6}$$

where $\vec{\Omega}$ is the angular velocity. Notice that for a rigid body, the position vector $\vec{r}$, is not a function of time and hence, $\dot{\vec{r}} = \ddot{\vec{r}} = 0$. Finally, the boundary condition for the temperature is obtained from the adiabatic boundary condition and is given by:

$$\left. \frac{\partial T}{\partial n} \right|_{wing} = 0 \tag{7}$$

COMPUTATIONAL SCHEME

The implicit, upwind, flux-difference splitting, finite-volume scheme is used to solve the unsteady, compressible, full Navier-Stokes equations. This scheme uses the flux-difference splitting of Roe and a smooth flux limiter is used to eliminate oscillation at locations of large flow gradients. The viscous and heat flux terms are linearized in time and the cross derivative terms are eliminated in the implicit operator and retained in the explicit terms. The viscous terms are differenced using second-order accurate central differencing. The resulting difference equation is approximately factored to solve the equations in three sweeps in the ξ^1, ξ^2, and ξ^3, directions. The computational scheme is coded in the computer program "FTNS3D".

The method of solution consists of three steps. In the first step, the problem is solved for the stationary wing at 0° roll angle. This solution represents the initial conditions for the second step. In the second step, the dynamic initial conditions are specified. A quarter cycle of a sinusoidal function is specified to roll the wing to a 10° roll angle with zero angular velocity while the Navier-Stokes equations are solved accurately in time. Having specified the dynamic initial conditions, the third step proceeds. Applying a four-stage Runge-Kutta scheme and the specified dynamic initial conditions for θ and $\dot{\theta}$, Eq. (4) is explicitly integrated in time in sequence with the fluid dynamic equations. Equation (4) is used to solve for θ, $\dot{\theta}$, and $\ddot{\theta}$ while the fluid dynamics equations provide the pressure distribution over the wing surface. The pressure distribution is integrated over the surface of the wing to determine $C_{m_{roll}}$, with respect to the axis of geometric symmetry. At each time step, the wing and the grid are rotated corresponding to θ and $\dot{\theta}$ resulting in the natural rolling response of the delta wing to the fluid flow. Due to the dynamic nature of the problem, the metric coefficients and the grid speed are computed at each time step. The computations proceed until periodic (limit cycle) response is reached.

RESULTS OF WING ROCK PROBLEM

In order to compare with available experimental data, an 80° swept-back, sharp-edged delta wing of zero thickness is considered for the subsonic flow solutions. This wing was modeled after the experimental model used by Arena[3]. An O-H grid of 65 x 43 x 84 in the wrap-around, normal, and axial directions, respectively, is used. The computational domain extends two chord lengths forward and five chord lengths backward from the wing trailing edge. The radius of the computational domain is four chord lengths. The minimum grid size in the normal direction to the wing surface is 5 x 10^{-4} from the leading edge to the plane of symmetry. The initial conditions correspond to the solution of the wing held at 30° angle of attack and 0° roll angle after 17,500 time steps at a Mach number and Reynolds number of 0.1 and 0.4 x 10^6, respectively.

From the initial conditions, this wing is forced to roll to an initial roll angle of θ = 10.0°. The wing is then released to respond to the fluid flow with a mass moment of inertial about the x– axis of the I_{xx} = 2.253 x 10^{-2}. Figure 1 shows the phase and time history of the resultant motion. From the initial displacement of θ = 10°, the wing oscillated in roll with a growing amplitude until periodicity is reached three cycles later. By t = 60, the motion is completely periodic with a maximum limit-cycle amplitude of 41.2°. For comparison, the experimental results for the same wing performed by Arena[3] showed a steady state amplitude of 41° at the same Reynolds number. Viewing the time histories of all three rotational properties, it is clear that the angular acceleration and roll angle are exactly 180° out of phase, while the angular velocity is nearly 90° out of pahse.

Figure 2 shows the time history of the lift coefficient and the phase of the periodic response of the rolling moment coefficient. Notice that the lift coefficient curve oscillates at twice the frequency of the wing motion. In the phase plot of the rolling moment coefficient, it is interesting to note the three lobes of the periodic response. These lobes represent the energy shift from the wing to the fluid in the outer two lobes as indicated by the "+" and from the fluid to the wing in the middle lobe as indicated by the "–". These outer lobes are referred to as damping lobes.

Figure 3 shows snapshots of a complete cycle of rolling depicting the total pressure contours at key points labeled in Figures 1 and 2. As the wing is approaching the maximum angular velocity, points g) to h) and j) to k), the footprint of the vortex core on the upward moving side appears to bow outward toward the leading edge of the wing. It appears that the eneven movement of the vortex core with respect to the leading edge is a result of the lagging movement of the fluid in response to the motion of the wing. Near the trailing edge, this effect is more pronounced due to the increased absolute velocity of the wing near the outer edges of the surface. When the fluid motion catches up to the motion of the wing, the energy flows from the fluid to the wing promoting the rolling motion, and stimulating wing rock. As the wing rolls, the angular velocity increases until the wing exceeds $\theta = \pm 27°$. Near the trailing edge, the absolute velocity of the wing exceeds the limit of the motion that the fluid can maintain. The flowfield reflects this lag by the bowed appearance of the vortex core. When the fluid flow motion lags the wing motion, energy is absorbed by the fluid providing damping to the system as indicated by the "+" in rolling moment phase diagram of Figure 2. As the wing slows, the cores appear to straighten and snap back. This effectively rolls the wing in the opposite direction.

FORMULATION OF ACTIVE CONTROL MODEL

The control system is developed using a space system representation. In this technique, the equations of motion are modeled in the form

$$\dot{x} = Ax + Bu \tag{8}$$

$$y = Cx + Du \tag{9}$$

where x is a vector of states, and u is a vector of external inputs. The matrices A, B, C, and D, define the character of the state equation, Eq. (8) and the measurement equation, Eq. (9). Since the initial system is the natural response of the wing to the fluid flow, there are no external inputs, therefore u = [0]. The equations of motion for the system which is free to roll only are:

$$\dot{\theta} = \frac{\partial \theta}{\partial t} \tag{10}$$

$$\ddot{\theta} = \frac{C_{m_{roll}}}{I_{xx}} \tag{11}$$

Note that Eq. (11) is the reduced form of Eq. (4) where $\omega_x = \dot{\theta}$ and $\dot{\omega}_x = \ddot{\theta}$ for the single degree of freedom system. The coefficient of rolling moment, $C_{m_{roll}}$, is determined from the flowfield by integrating the pressure over the surface of the wing. For the given freestream conditions, the pressure distribution is a function of θ, $\dot{\theta}$, and to a much lesser extent various other parameters defined by the strength and location of the vortices. Since an exact relationship for the pressure distribution is undetermined, it is necessary to develop an estimator for the system. by developing a reduced order estimator, a state-space model can be developed in such a way that the dynamics of the system are preserved. With this reduction, the estimator is a function of only the controllable states, θ, $\dot{\theta}$.

Reduced Order Model

Since an explicit formulation for the pressure distribution is unobtainable, a reduced order balanced realization can only be estimated. From the data of the free-to-roll case, Fig. 1, an equation is formulated to estimate $\ddot{\theta}$ as a function of θ and $\dot{\theta}$. Using a multiple regression for the two carriers, θ and $\dot{\theta}$, the resulting nondimensional estimated equation of motion is as follows:

$$\ddot{\theta} = -0.0777\,\theta \tag{12}$$

Noting the response of the wing motion, it is not surprising that the estimated reduced order system resembles an undamped linear oscillator. Comparison of the estimated dynamic system with the actual system is shown in Fig. 4. The estimated response has less than 4% error when compared to the actual nondimensional angular acceleration. For the purpose of this investigation, this estimator is deemed an appropriate choice to model the actual system. The estimated reduced order system in state-space representation, Eqs. 8 and 9, yields the following:

$$\begin{aligned} x &= \begin{bmatrix} \theta \\ \dot{\theta} \end{bmatrix} \quad u = [0] \quad y = \begin{bmatrix} \theta \\ \dot{\theta} \end{bmatrix} \\ A &= \begin{bmatrix} 0 & 1 \\ -0.0777 & 0 \end{bmatrix} \quad B = \begin{bmatrix} 0 \\ 0 \end{bmatrix} \\ C &= \begin{bmatrix} 1 & 0 \\ 0 & 1 \end{bmatrix} \quad D = \begin{bmatrix} 0 \\ 0 \end{bmatrix} \end{aligned} \tag{13}$$

The dynamic response of the model based on the eigenvalues, places the open loop poles at $S_{1,2} = \pm\sqrt{-0.0777}$.

Feedback Control

Using a state feedback control, the system can be diagrammed as shown in Figure 5. With feedback control, the system of equations are:

$$\dot{\theta} = \frac{\partial \theta}{\partial t} \tag{14}$$

$$\ddot{\theta}_c = -0.0777\theta + \frac{1}{I_{xx}}u \tag{15}$$

Where $C_{m_{roll_c}} = I_{xx}\ddot{\theta}_c$ is the controlled moment function and u is the external control moment input. In state-space representation, Eqs. (14) and (15) are of the following form:

$$\begin{aligned} x &= \begin{bmatrix} \theta \\ \dot{\theta} \end{bmatrix} \quad u = -Gx \quad y = \begin{bmatrix} \theta \\ \dot{\theta} \end{bmatrix} \\ A &= \begin{bmatrix} 0 & 1 \\ -0.0777 & 0 \end{bmatrix} \quad B = \begin{bmatrix} 0 \\ \frac{1}{I_{xx}} \end{bmatrix} \\ C &= \begin{bmatrix} 1 & 0 \\ 0 & 1 \end{bmatrix} \quad D = \begin{bmatrix} 0 \\ 0 \end{bmatrix} \quad G = [g_1 \quad g_2] \end{aligned} \tag{16}$$

From this system, the appropriate gain matrix, G, can be determined from the formula of the closed loop dynamics matrix:

$$A_c = A - BG \tag{17}$$

Where the characteristic equation of A_c must satisfy the Butterworth polynomial. Solving for the characteristic equation of Eq. (17) yields:

$$S^2 + \frac{g_2}{I_{xx}}S + \left(\frac{g_1}{I_{xx}} + 0.0777\right) = 0 \tag{18}$$

The value of the damping for the control system, ω_0, is set equal to 4.44 to obtain an acceptable response time without requiring unrealistic control energy. This also ensured that the order of magnitude of the control matrix, BG, was sufficiently large to eliminate any adverse effects due to errors resulting from the estimated model. Therefore, the desired characteristic equation according to the Butterworth configuration is:

$$S^2 + \sqrt{2}\omega_0 S + \omega_0^2 = 0 \tag{19}$$

Matching coefficients yields the gain matrix, G, and control law as follows:

$$G = [0.4424 \quad 0.1416] \tag{20}$$

$$u = -0.4424\,\theta - 0.1416\,\dot{\theta} \tag{21}$$

Solution Methodology

To impart the rolling moment required by the control law specified in Eq. (21), a mass injection system is developed. On both the upper and lower surfaces of the wing, areas aft of the pitch axis and near the leading edge were designated for control. Figure 6 shows these areas as dark shaded regions on the wing surface. The boundary condition for the wing surface was then modified to reflect the velocity being imparted by the fluid of the control system on the wing. By using both upper and lower surfaces and blowing and suction of fluid, the effective region for control was quadrupled.

RESULTS FOR ACTIVE CONTROL MODEL

Initial Conditions

The initial conditions for the active control application correspond to the results of the wing rock case. Specifically, to demonstrate the effectiveness of the control design, a time when the wing was at the maximum roll angle was chosen for the initial conditions. By time t = 92.3, the wing has rolled to 41.1° and exhibits a very small negative angular velocity. This time corresponds to the results of point f) in Fig. 1.

Response History

With the control system applied, the flowfield is resolved and the response of the wing determined. Figure 7 shows plots of the time history and phase of the motion. For comparison, the response of the uncontrolled wing motion is shown with a dashed and dotted line. Within one and one half cycles, the wing is brought to rest at a roll angle and a roll velocity of 0°.

Figure 8 is a plot of the nondimensional velocity of the fluid mass injected into the flow. For convention, a positive velocity indicates that fluid is being blown into the flowfield. A negative velocity indicates that fluid is being sucked away from the flowfield. As the control surfaces are on both sides of the wing, all references to the direction of the fluid are made with respect to the upper surface of the right side of the wing. Hence, a positive velocity indicates that mass is blowing into the flow on the upper right side surface and lower left side and mass is sucked away from the flow on the lower right side surface and upper left side.

By t = 130.0, the wing is essentially at rest. Constraint of computational resources limited continuation of this case. Figure 9 shows the Mach number and pressure contours of the wing surface. While the Mach contours indicate that the control system is still actively preventing any rolling motion, the pressure contours show a strong similarity to the initial conditions of the flowfield before motion is imposed on the wing.

In Figure 10, it is clear that the flowfield is almost symmetric. There is no breakdown of the primary vortex cores and the flow appears to be stable.

CONCLUDING REMARKS

A control system was developed to control the phenomenon of wing rock. Based on a reduced order estimation of the system, the control problem was reduced to a second order problem for efficient and effective computer usage. Using pole placement techniques, a control law was determined in order to produce a stable system based on state feedback. Application of the designed control law incorporated a mass injection system from four areas on the wing surface. Imparting mass into the flowfield according to the established control law produced a restoring moment with the appropriate phase lag. This mass injection system also affected the features of the flow field providing additional damping to the system. The aim of this control system was to eliminate the wing motion and return the wing to the zero roll angle of the initial conditions.

To demonstrate the effectiveness of the design, the control system was applied to a delta wing undergoing a rock after a periodic response was achieved at t = 92.3. At this point, the wing is near the peak value of roll angle with a slight negative roll velocity. Injecting fluid into the flow on the left side, the wing motion is immerdiately reduced. Since the control law is based on the feedback of two states, the roll angle and roll velocity, the system automatically has the necessary phase lag in order to prevent divergence of the wing motion. Due to the injection of fluid, the vortex core on the left side of the wing eventually breaks down. As has been established in Reference 17, the breakdown of the vortex is beneficial to control since the breakdown provides additional damping to the system.

Within one and one half cycles at a reduced period of oscillation, the wing is essentially brought to rest with $\theta \approx 0°$. The designed control system achieves the desired result and the flowfield appears to be stable.

ACKNOWLEDGMENT

This work is supported by the NASA-Langley Research Center under grant No. NAG-1-648 along with partial support from the Virginia Space Grant Consortium. The computational resources provided by the NAS Center at AMES and the NASA Langley Research Center are acknowledged and appreciated.

REFERENCES

1. Nguyen, L. E., Yip, L. P., and Chambers, J. R., "Self Induced Wing rock of Slender Delta Wings," AIAA Paper No. 81–1883, August, 1981.

2. Ericsson, L. E., "thir Fluid Mechanics of Slender Wing Rick, "*Journal of Aircraft*, Vol. 21, No. 5, 1984, pp. 322–328.

3. Arena, A. S., *An Experimental and Computational Investigation of Slender Wings Undergoing Wing Rock*, Ph.D. Dissertation, University of Notre Dame, April, 1992.

4. Ng, T. T., Malcolm, G. N., and Lewis, L. C., "Experimental Study of Vortex Flows over Delta Wings in Wing-Rock Motion," *Journal of Aircraft*, Vol. 29, No. 4, July-August, 1992.

5. Malcolm, G. N., Ng, T. T., Lewis, L., and Murri, D. G., "Development of Non-Conventional Control Methods for High Angle of Attack Flight Using Vortex Manipulation," AIAA Paper No. 89–2192, July, 1989.

6. Walton, J. and Katz, J., "Application of Leading-Edge Vortex Manipulations to Reduce Wing Rock Amplitudes," *Journal of Aircraft*, Vol. 30, No. 4, July-August, 1993.

7. Ng, T. T., Skaff, T., and Kountz, J., "Effect of Leeward Flow Divider on the Wing Rock of a Delta Wing," *Journal of Aircraft*, Vol. 31, No. 6, November-December, 1994.

8. Wong, G. S., Rock, S. M., Wood, N. J., and Roberts, L., "Active Control of Wing Rock Using Tangential Leading-Edge Blowing," *Journal of Aircraft*, Vol. 31, No. 3, May-June, 1994.

9. Konstadinopoulos, P., Mook, D. T., and Nayfeh, A. H., "Subsonic Wing Rock of Slender Delta Wings," *Journal of Aircraft*, Vol. 22, No. 3, March, 1985.

10. Nayfeh, A. H., Elzebda, J. M., and Mook, D. T., "Analytical Study of the Subsonic Wing-Rock Phenomenon for Slender Delta Wings," *Journal of Aircraft*, Vol. 26, No. 9, September, 1989.

11. Chaderijian, N. M. and Schiff, L. B., "Navier-Stokes Prediction of Large-Amplitude Forced and Free-toRoll Delta-Wing Oscillations," AIAA Paper No. 94–1884-CP, 1994.

12. Kandil, O. A. and Salman, A. A., "Effects of Leading-Edge Flap Oscillation of Unsteady Delta Wing Flow and Rock Control," AIAA Paper No. 91–1796, June, 1991.

13. Kandil, O. A. and Salman, A. A., "Prediction and Control of Slender Wing Rock," ICAS 92–4.7.2, 1992, pp. 1430–1441.

14. Kandil, O. A. and Salman, A. A., "Recent Advances in Unsteady Computations and Applications of Vortex Dominated Flows," 4th International Symposium on computational Fluid Dynamics, Davis, CA, September, 1991, pp. 570–575.

15. Salman, A. A., *Unsteady Euler and Navier-Stokes Computations Around Oscillating Delta Wing including dynamics*, Ph.D. Dissertation, Old Dominion University, April, 1992.

16. Lee-Rausch, E. M. and Batina, J. T., "Conical Euler Analysis and Active Roll Suppression for Unsteady Vortical Flows about Rolling Delta Wings," NASA Technical Paper 3259, 1993.

17. Menzies, M. A. and Kandil, O. A., "Natural Rolling Responses of a Delta Wing in Transonic and Subsonic Flows," AIAA-96–3391–CP AIAA Atmospheric Flight Mechanics Conference, San Diego, CA, July 29–31, 1966, pp. 246–254.

18. Kandil, O. A. and Kandil, H. A., "Pitching Oscillation of a 65–Degree Delta Wing in Transonic Vortex Breakdown Flow," AIAA-94–1426–CP, AIAA/ASME/ASCE/AHS/ASC Structures and Structural Dynamics conference, Hilton Head, SC, April 18-20, 1994, pp. 995–966.

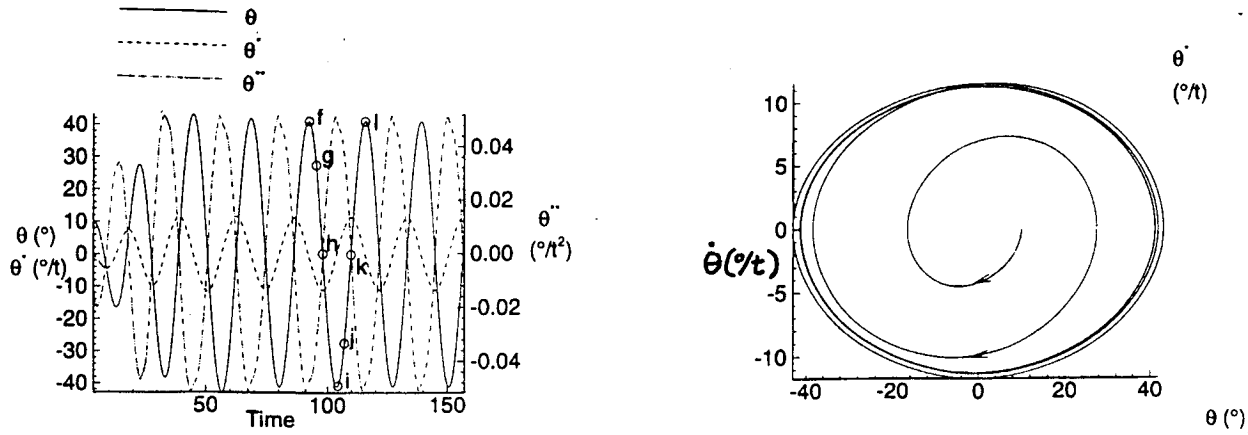

Figure 1. Time History of Roll Angle, θ, Angular Velocity, $\dot{\theta}$, Angular Acceleration, $\ddot{\theta}$ and Phase of Angular Velocity, $\dot{\theta}$, $M_\infty = 0.1$, $Re = 0.4x10^6$, $\alpha = 30.0^o$, $\theta_{ic} = 10.0^o$, $\dot{\theta}_{ic} = 0.0^o/t$ (with points of interest annotated).

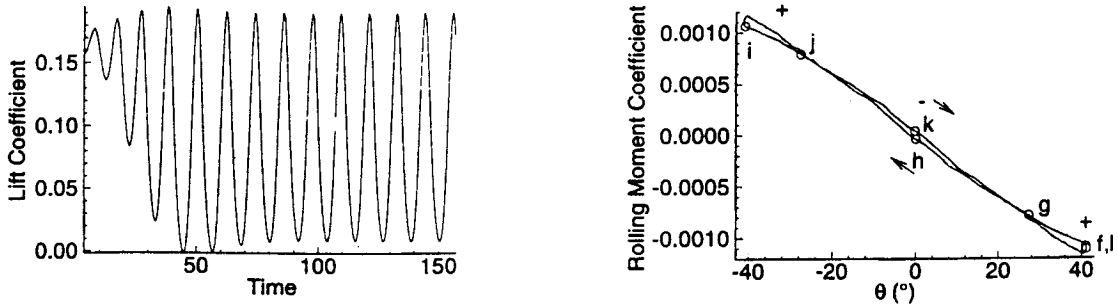

Figure 2. Time History of Lift Coefficient and Phase of Rolling Moment Coefficient indicating Energy Transfer Lobes. (with points of interest annotated).

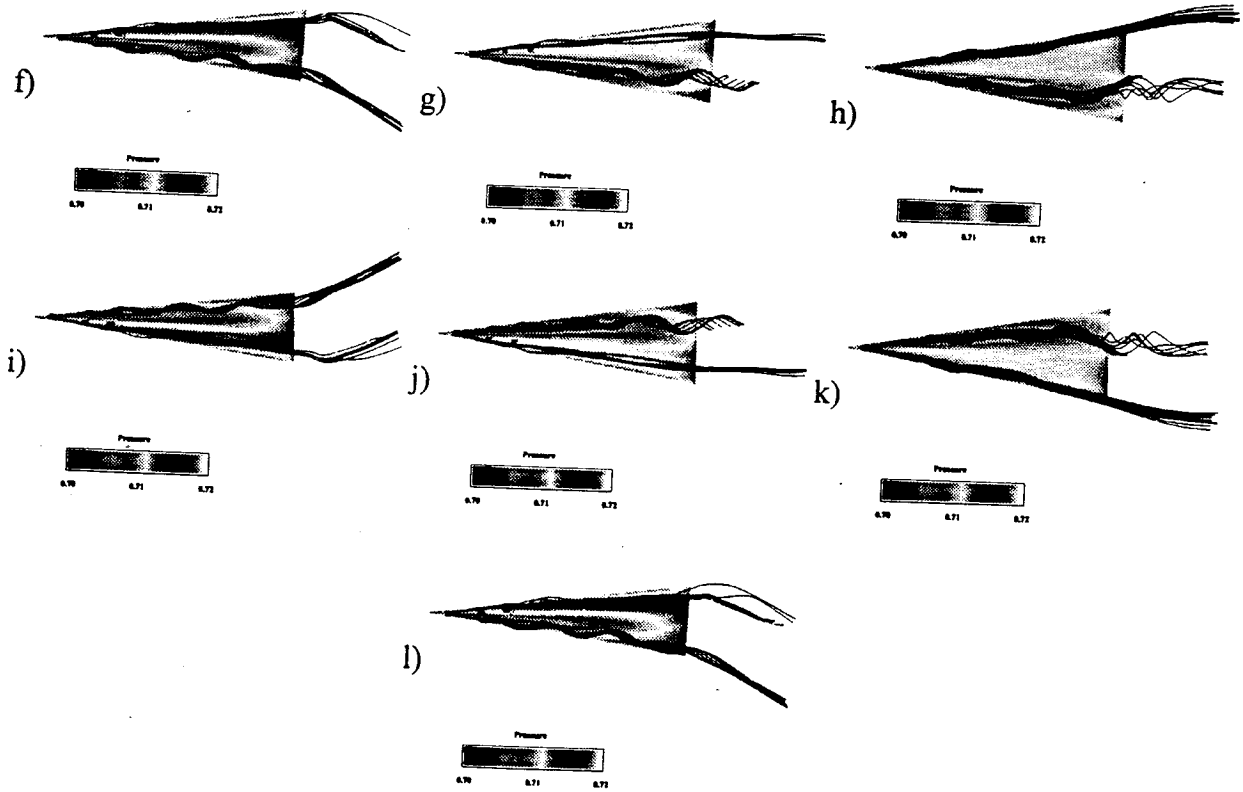

Figure 3. Snapshots of a Complete Cycle of Rolling Oscillation depicting the Total Pressure Contours at Points of Interest at $f)\theta = 41.1^o, g)\theta = 27.3^o, h)\theta = 0.0^o\, i)\theta = -40.8^o$, $j)\ \theta = -27.5^o$, $k)\ \theta = -0.2^o$, $l)\ \theta = 41.2^o$.

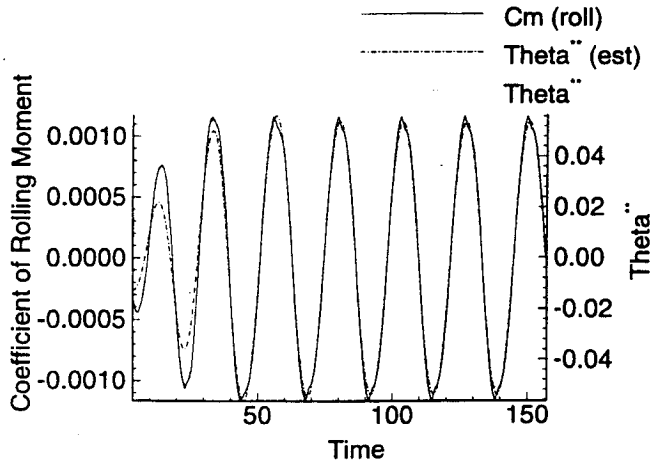

Figure 4. Comparison of the Computed Coefficient of Rolling Moment and Nondimensional Angular Acceleration with the Estimated Dynamic System Response Plotted vs. Time.

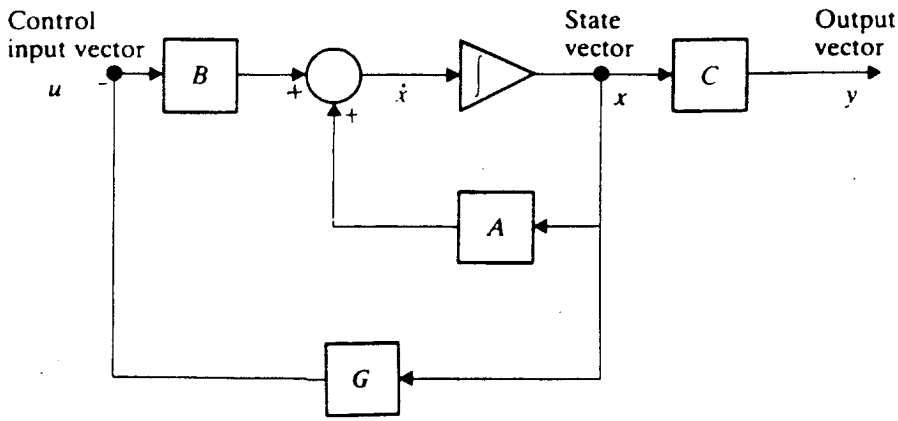

Figure 5. Block-diagram Representation of the Feedback Control system.

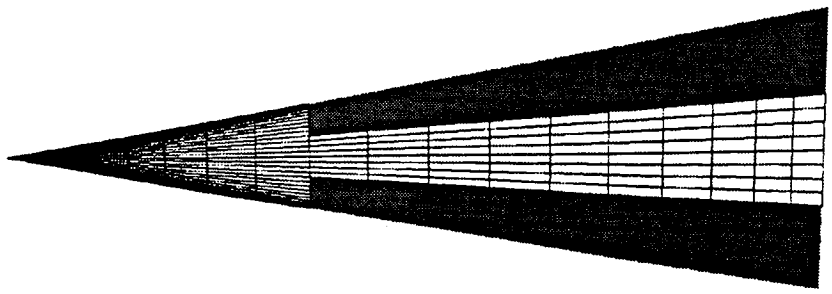

Figure 6. Control Regions on the Wing Surface.

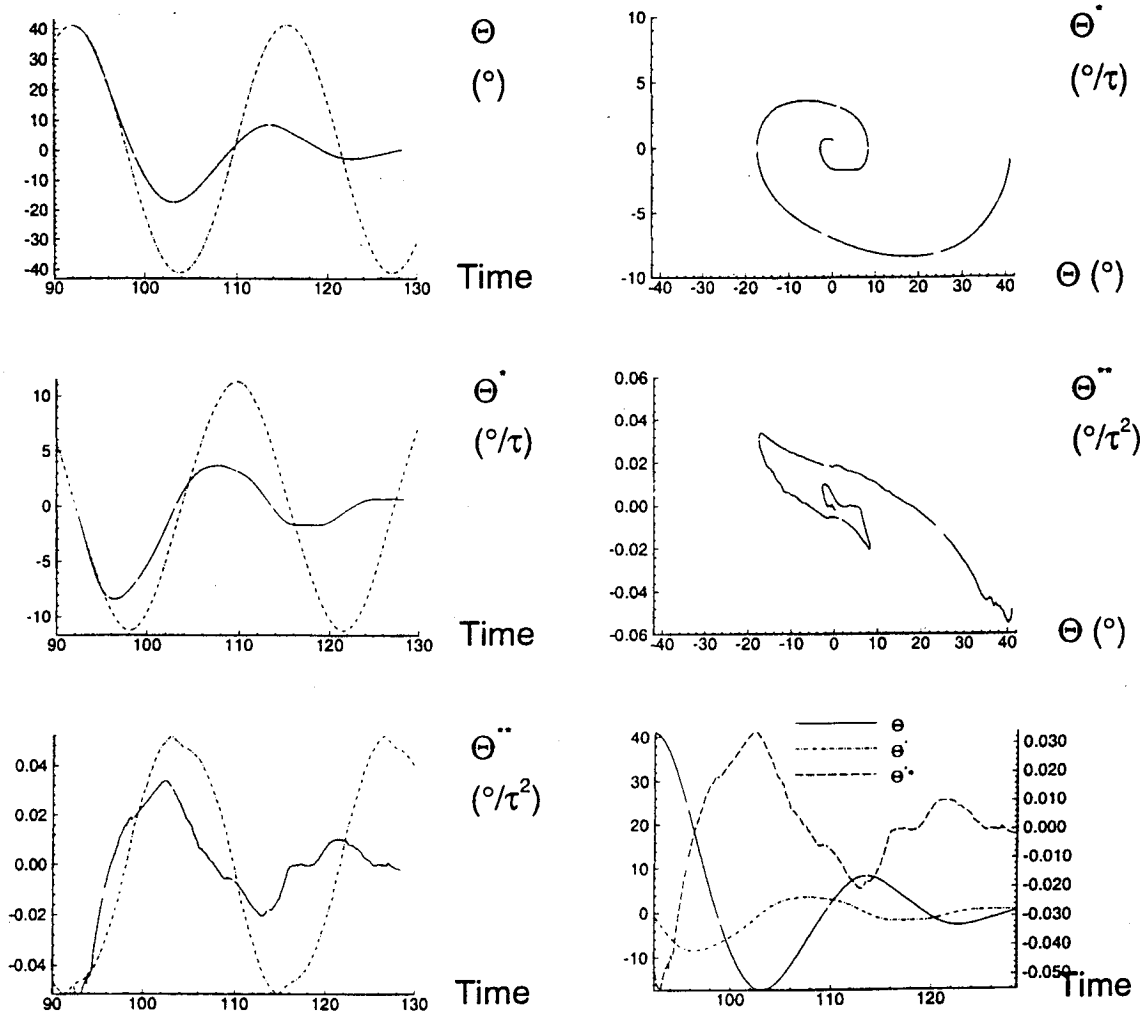

Figure 7. Time History and Phase Plots of the Response after Active Control is Applied.

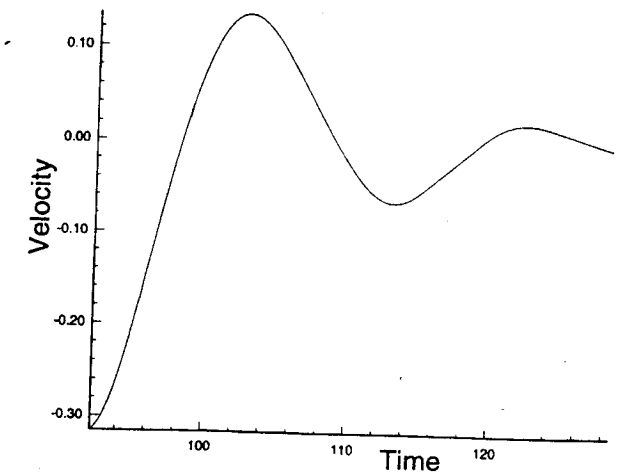

Figure 8. Plot of the Nondimensional Velocity of the Mass Injected into the Flow (right-upper surface).

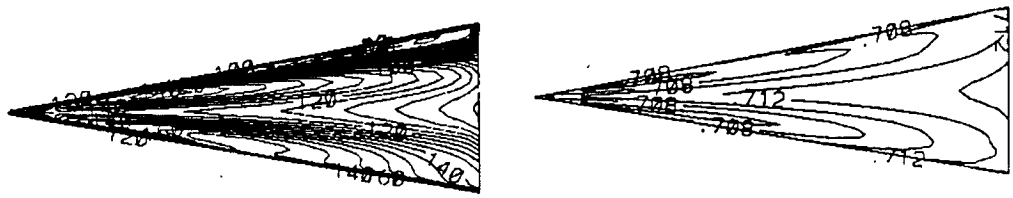

Figure 9. Total Mach Number Contours near the Wing Surface and Pressure Contours on the Wing Surface at $\theta \approx 0^o$.

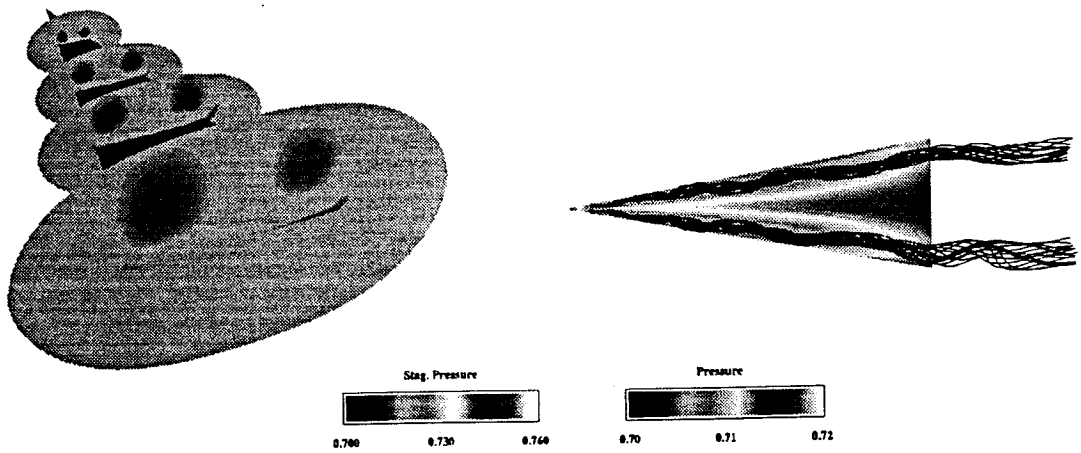

Figure 10. Total Pressure Contours on Cross-Flow Planes and on the Wing Surface with Instantaneous Streamlines.

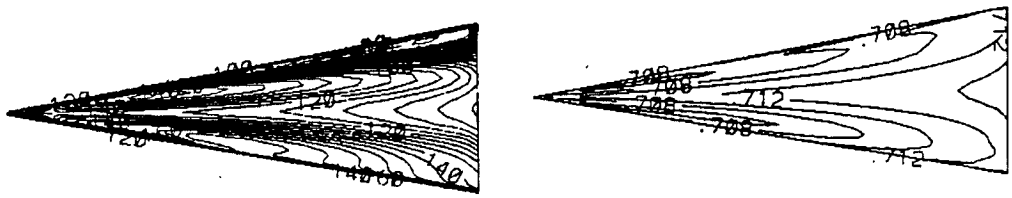

Figure 9. Total Mach Number Contours near the Wing Surface and Pressure Contours on the Wing Surface at $\theta \approx 0^o$.

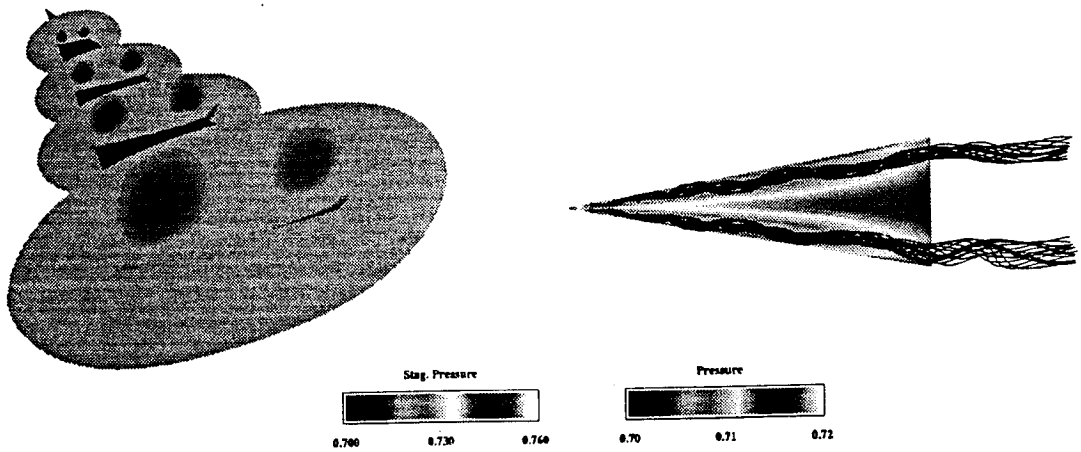

Figure 10. Total Pressure Contours on Cross-Flow Planes and on the Wing Surface with Instantaneous Streamlines.